Journal of Structural Geology 38 (2012) 51–60

Contents lists available at SciVerse ScienceDirect

Journal of Structural Geology

journal homepage: www.elsevier.com/locate/jsg

Correlation of clayey gouge in a surface exposure of serpentinite in the San Andreas Fault with gouge from the San Andreas Fault Observatory at Depth (SAFOD)

Diane E. Moore*, Michael J. Rymer

U.S. Geological Survey, Earthquake Science Center, 345 Middlefield Road, Mail Stop 977, Menlo Park, CA 94025, USA

ARTICLE INFO

Article history:
Received 15 April 2011
Received in revised form
4 November 2011
Accepted 23 November 2011
Available online 6 December 2011

Keywords:
San Andreas Fault
SAFOD
Serpentinite
Metasomatic reactions
Saponitic smectite clays
Coast Range Ophiolite

ABSTRACT

Magnesium-rich clayey gouge similar to that comprising the two actively creeping strands of the San Andreas Fault in drill core from the San Andreas Fault Observatory at Depth (SAFOD) has been identified in a nearby outcrop of serpentinite within the fault zone at Nelson Creek. Each occurrence of the gouge consists of porphyroclasts of serpentinite and sedimentary rocks dispersed in a fine-grained, foliated matrix of Mg-rich smectitic clays. The clay minerals in all three gouges are interpreted to be the product of fluid-assisted, shear-enhanced reactions between quartzofeldspathic wall rocks and serpentinite that was tectonically entrained in the fault from a source in the Coast Range Ophiolite. We infer that the gouge at Nelson Creek connects to one or both of the gouge zones in the SAFOD core, and that similar gouge may occur at depths in between. The special significance of the outcrop is that it preserves the early stages of mineral reactions that are greatly advanced at depth, and it confirms the involvement of serpentinite and the Mg-rich phyllosilicate minerals that replace it in promoting creep along the central San Andreas Fault.

Published by Elsevier Ltd.

1. Introduction

A tectonic shear zone of serpentinite 3–50 m in width that extends for at least 4–5 km within the San Andreas Fault (SAF) was identified during geologic mapping of the area surrounding the proposed SAFOD drill site near Parkfield, California (Fig. 1A). This portion of the SAF is situated within the central creeping section, characterized by a creep rate of ~25 mm/yr (Titus et al., 2006). A rare ~3 m wide outcrop of the serpentinite, exposed in Nelson Creek about 2.4 km NNE of the SAFOD drill site, was sampled extensively (Fig. 1B). At this locality the serpentinite is faulted against Tertiary sandstones and siltstones on both sides; the fault trace on the northeast side of the serpentinite fractured during the 2004 Parkfield earthquake (Rymer et al., 2006). One curious sample collected from a black, fine-grained zone about 0.15 m wide and 0.5 m long at the fault contact (Fig. 1B) consists of fragments of serpentinite and sedimentary rock distributed in a foliated, clay-rich matrix. The significance of this sample became clear when similar phyllosilicate-rich fault gouge containing serpentinite porphyroclasts was recovered at two depths in the Phase 3 SAFOD core, corresponding to the places where the well casing of the main borehole is deforming in response to fault creep (Zoback et al., 2010).

The main drill hole at SAFOD, completed in two phases, followed the trajectory sketched in Fig. 1A (Zoback et al., 2010). Drilling began in Salinian granitic rocks and arkosic sediments of the Pacific plate and terminated in Great Valley Group sedimentary rocks of the North American plate. Phase 3 coring operations in 2007 focused on the two positions of well casing deformation identified at true vertical depths of ~2.65 and ~2.7 km (Fig. 1C) and temperatures of 112–114 °C. The 2.6 m wide central deforming zone (CDZ) (Zoback et al., 2010) is situated near the middle of the 200 m wide damage zone of the currently active fault, and it evidently is accommodating most of the creep based on the pronounced casing deformation associated with it. The CDZ extends from 3296.6 to 3299.1 m measured depth (MD) in Phase 3 Hole G. The less active, 1.6 m wide southwest deforming zone (SDZ, 3196.4–3198.1 m MD) marks the southwestern margin of the SAF damage zone (Fig. 1C) (Zoback et al., 2010). Variably deformed shales, siltstones, and fine-grained sandstones adjoin both gouge zones. Bradbury et al. (2011) and Holdsworth et al. (2011) present overviews of the entire set of Phase 3 core. Bradbury et al. (2011) emphasize mesoscale lithologic and

* Corresponding author. Tel.: +1 650 329 4825; fax: +1 650 329 5143.
E-mail addresses: dmoore@usgs.gov (D.E. Moore), mrymer@usgs.gov (M.J. Rymer).

0191-8141/$ – see front matter Published by Elsevier Ltd.
doi:10.1016/j.jsg.2011.11.014

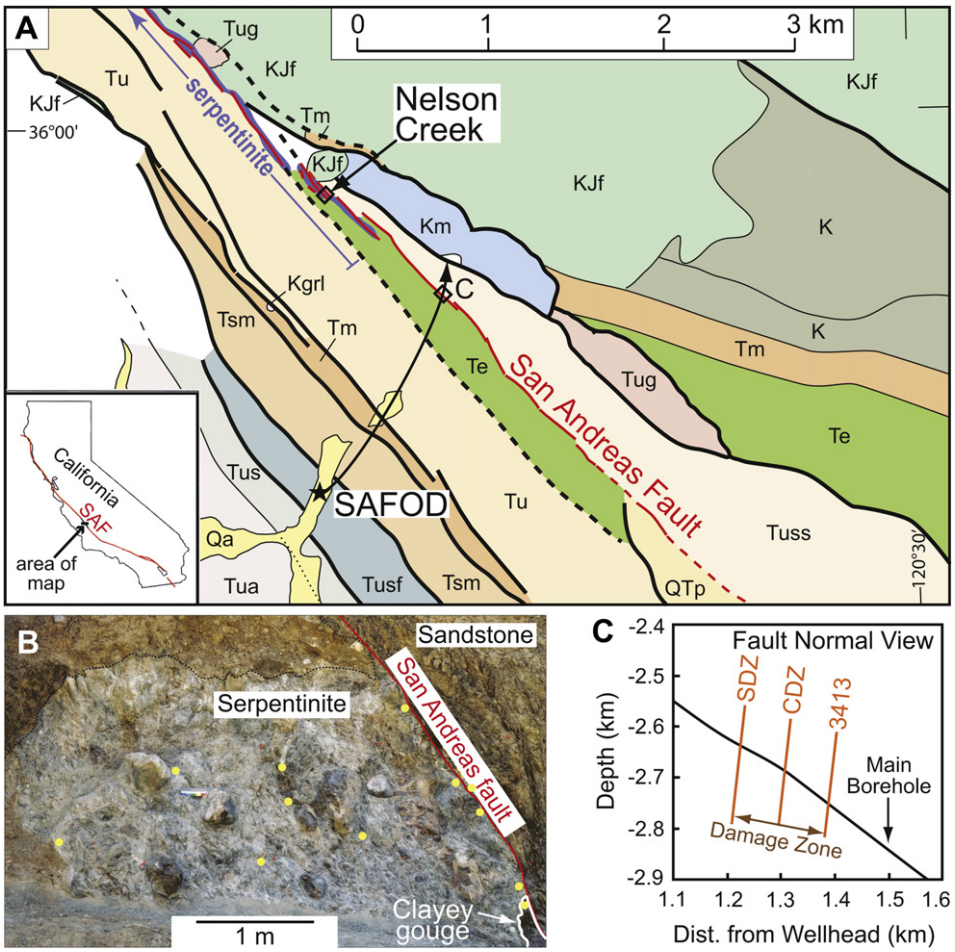

Fig. 1. (A) Geologic map of the area around the Nelson Creek serpentinite outcrop and SAFOD drill site. Serpentinite occurs as a tectonic smear within the fault zone and extends for at least 2–2.5 km to the northwest of the mapped area (extent indicated by purple arrow). The curved black arrow extending northeast from the SAFOD drill site is the approximate path of the drill hole at depth (box labeled C is the location of Fig. 1C). Rock units: purple, serpentinite; KJf, Franciscan Complex; K, Great Valley Group; Km, Cretaceous (?) marble; Kgrl, granite sliver; Te, Etchigoin Formation; Tm, Monterey Shale; Tsm, Santa Margarita (?) Formation; Tu, unnamed mudstone; Tua, unnamed sandstone, volcanic ash rich; Tug, unnamed conglomerate with granitic detritus; Tus, unnamed sandstone, to mudstone; Tusf, unnamed sandstone with Franciscan cobbles; Tuss, unnamed sandstone, siltstone; QTp, Paso Robles Formation; Qa, alluvium. The main trace of the currently active SAF is drawn in red; other faults are mapped as heavy black lines, dashed where inferred. (B) Photograph of the outcrop at Nelson Creek, showing serpentinite faulted against Tertiary sandstone; clayey gouge abuts the fault trace that fractured during the 2004 Parkfield earthquake (Rymer et al., 2006). Yellow dots mark sample locations. (C) Cross-sectional view, looking to the northwest, of the SAFOD borehole showing the locations of the CDZ and SDZ relative to the damage zone of the currently active fault (simplified from Fig. 1C of Zoback et al., 2010).

structural features, whereas Holdsworth et al. (2011) provide petrographic and microstructural observations using the thin section set from the Phase 3 Core Atlas (http://www.earthscope.org).

In this paper, we present a preliminary textural and mineralogical description of the Nelson Creek (NC) fault gouge and compare it to core samples of the foliated gouge from the CDZ and SDZ. We show that all three gouges have the same general characteristics and conclude that they formed by the same processes of shear-enhanced reaction of serpentinite with crustal rocks. The compositions of chromian spinels (e.g., Dick and Bullen, 1984) further suggest that the serpentinites in the three occurrences may have a common source in the Coast Range Ophiolite. The tectonic implications of the correlation of the NC gouge with those at depth are discussed.

2. Methods

This study is largely based on examination of polished thin sections. Preliminary observations were made using an optical microscope. However, because many of the samples are very fine-grained, much of the petrographic work was conducted on a scanning electron microscope (SEM) equipped with an energy dispersive spectrometer (EDS). The EDS capability was used to aid in mineral identifications, provide qualitative information on mineral chemistry, and map element distributions at two locations in the NC gouge. Mineral identifications were augmented by X-ray diffraction (XRD) analysis of powdered rock samples.

Quantitative chemical analyses of gouge-matrix clays, serpentine minerals, and spinels were made with an electron probe microanalyzer (EPMA) at conditions of 15 kV accelerating voltage and 10 nA beam current. The mineral standard set consists of feldspars (Si, Al, Ca, Na, K), natural olivines (Mg, Fe, Ni), chromite (Cr), and the oxides Mn_2O_3 (Mn) and TiO_2 (Ti). A set of mineral standards was also tested at intervals during the runs, to check for drift in sample current. A 10 μm beam diameter was used initially because of concerns that the water-rich clays and serpentine minerals might be damaged by a more focused beam. Following some comparative tests using different spot sizes, a beam diameter of 5 μm has now been adopted.

Even the smaller spot diameter used for microprobe analysis is larger than the grain size of many of the minerals in the gouge matrix. Because of this, a given spot analysis of the matrix clays might represent at best a polycrystalline aggregate of the same mineral, along with some intervening pore space that lowers the anhydrous total. Alternatively, a given composition could represent mixed-layer phyllosilicates of various kinds or a physical mixture of clay minerals with calcite, quartz, feldspar, or other minerals. Difficulties in achieving a good polished surface on thin sections of the gouge can also result in low anhydrous totals. At least half the data collected from the samples of gouge matrix were discarded because of low totals, obvious contamination, or unreasonable calculated structural formulas.

3. Petrography and mineral chemistry

3.1. Nelson Creek serpentinite

The serpentinite portion of the NC outcrop (the yellow dots in Fig. 1B mark the sample locations) consists of resistant blocks of thoroughly serpentinized ultramafic rock dispersed in a bluish-gray, sheared serpentinite matrix, corresponding to the serpentinite "broken formation" of Shervais et al. (2005). With the exception of euhedral crystals of brownish-red to nearly opaque spinel, no relict primary minerals were seen. All three principal serpentine minerals — antigorite, lizardite, and chrysotile — were identified in XRD patterns. The sample containing the largest proportion of antigorite (Supplementary Fig. 1A) comes from a resistant block in the center of the outcrop. The serpentinite in that block appears undeformed, and bands of fine-grained magnetite outline the boundaries of the original ultramafic minerals (Fig. 2A). Much of the bladed serpentine within a single primary crystal shows a strong preferred orientation, which varies from grain to grain. In many places, fan-shaped bundles or sprays of serpentine overprint the bladed texture (Fig. 2A).

The other samples show varying degrees of brecciation and shearing of serpentinite with mesh and bastite textures (Fig. 2B–D), and the proportions of lizardite and chrysotile are considerably higher relative to antigorite. In Fig. 2B, some reasonably well preserved mesh texture is at lower right, becoming progressively more flattened in the direction of the bastite at upper left. In the more strongly sheared samples, fragments of mesh and bastite texture serpentine as well as veins are dispersed in a fine-grained, foliated serpentinite matrix (Fig. 2C–D).

Brucite was identified in several samples on the basis of XRD analysis (Supplementary Fig. 1B) and SEM observations. It typically is a minor component disseminated in the serpentinite, but in one occurrence a brucite-rich rind surrounds a resistant block of serpentinite. The brucite is variably altered to pyroaurite ± coalingite (Supplementary Fig. 1B), which form when brucite is exposed to air (Mumpton et al., 1965; Mumpton and Thompson, 1966). Brucite is present in all six samples collected from the interior of the serpentinite outcrop, but neither it nor any of its weathering products was identified in XRD patterns of the samples collected along the fault boundary (Fig. 1B). The distribution of calcite is inversely correlated with that of brucite; no calcite was found in the samples from the interior of the block, but it is very abundant in those adjacent to the fault. These mineral distributions suggest that the serpentinite has very low permeability overall and that interaction of the serpentinite with local groundwaters was restricted to the faulted boundary (e.g., Hostetler et al., 1966; Mumpton and Thompson, 1966).

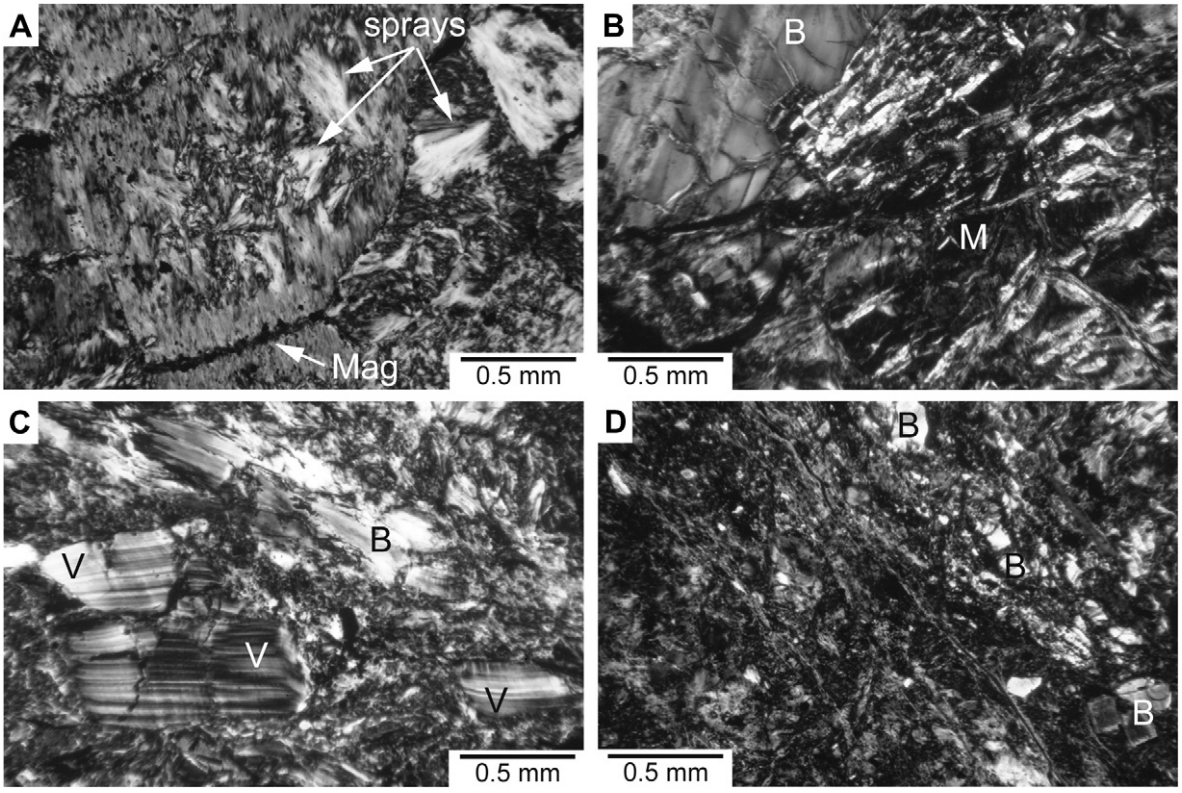

Fig. 2. Photomicrographs (crossed polarizers) of serpentinite textures from Nelson Creek. (A) Block of undeformed serpentinite from center of outcrop. The edges of former primary minerals are dotted with magnetite (Mag; abbreviations of common mineral names are from Whitney and Evans, 2010). Much of the serpentine forms randomly oriented sprays of crystals. (B) Slightly deformed bastite (B, upper left) and mesh (M, lower right) textures. (C) Fragments of bastite and possible serpentine veins (V) in a sheared serpentinite. (D) Highly sheared serpentinite; small pieces of bastite are translated parallel to the foliation.

3.2. Fault gouge occurrences

The NC, CDZ, and SDZ gouges have many similarities in texture and mineralogy and will be described together. The single NC gouge sample was situated very close to the boundary with the SAF (Fig. 1B). Four samples of the foliated gouge from the Phase 3 SAFOD core are described here, one from the SDZ and three from the CDZ. The SDZ sample was collected at 3197.7 m MD. Two of the CDZ samples come from the interior of the gouge zone at 3297.5 and 3298.6 m MD; the third straddles the gouge-siltstone contact marking the southwest boundary of the CDZ (3296.6 m MD).

Each gouge consists of porphyroclasts of serpentinite and other, predominantly sedimentary rock types dispersed in a foliated, clay-rich matrix (Fig. 3). The largest porphyroclast is a ~30 cm long boulder of serpentinite in the SDZ (Phase 3 Core Atlas and Fig. 7 of Bradbury et al., 2011). Most of the porphyroclasts are elongate and typically occur in a subparallel alignment (Sills et al., 2009; Chester et al., 2010). Some have rounded edges suggestive of mechanical wear, whereas others have tapered ends that may result from a combination of shearing and chemical alteration (e.g., Sills et al., 2009) (Figs. 3 and 4A). Some grains, such as the serpentinite porphyroclast in Fig. 4A, are slightly offset along transgranular fractures. Micron-scale clasts are abundant in the gouge matrix (Fig. 4B).

The serpentine mineral varieties lizardite and chrysotile, but not antigorite, were identified in powder XRD patterns of serpentinite porphyroclasts in the CDZ and SDZ (see also Bradbury et al., 2011). The larger serpentinite porphyroclast from the CDZ shown in Fig. 3B does contain the alteration assemblage talc + tremolite/actinolite + chlorite ± andradite garnet (Fig. 4C). One or more of these minerals appears in numerous other serpentinite porphyroclasts and as separate grains (Fig. 4D) in both the SDZ and CDZ samples. The talc-tremolite-chlorite assemblage typically forms in antigorite-bearing serpentinite, usually at greenschist facies conditions (e.g., Sanford, 1982) but also, in a few cases, at temperatures in the range 200–300 °C (e.g., Soda and Takagi, 2010).

The clays comprising the matrix of the NC, CDZ, and SDZ gouges are all Mg-rich, as determined initially by EDS measurements (see also Holdsworth et al., 2011). The porphyroclasts are variably altered to the same Mg-rich clays at their outer edges and along internal fractures. For example, Mg clays are interspersed with serpentine minerals in a ~200 μm wide band at the rim of the porphyroclast in Fig. 4C. Similarly, the fractures in a volcanic clast consisting largely of quartz + plagioclase + titanite (Fig. 4E) are all filled with Mg clays. The siltstone unit on the southwest side of the CDZ (Fig. 4F) is heavily fractured along the contact (Fig. 4F), and the fractures are lined with the same Mg-rich clays as those that characterize the gouge matrix (Fig. 4F and G).

Holdsworth et al. (2011) noted that in the actively creeping strands of the SAFOD core, veins of calcite or other minerals are restricted to the interiors of porphyroclasts, the vein minerals occurring only as rounded clasts in the gouge matrix. Textures of the NC, CDZ and, for the most part, SDZ samples examined in this study are consistent with their observations. This is illustrated in Fig. 4B, where nearly all of the tiny, bright flecks in the gouge matrix are calcite. However, narrow calcite veinlets ≤5 mm in length are found in the foliated matrix of the more slowly deforming SDZ (Fig. 4H). In a few of these veinlets, small amounts of Mg clays appear to have precipitated along with the calcite.

X-ray maps of Mg and Al (Fig. 5) were obtained at two places along the boundary between the large shale fragment and the gouge matrix in the NC sample (Fig. 3A). Brightness in these images increases with increasing concentration of a given element. The scans illustrate the intermediate Mg and Al contents of the clayey gouge matrix relative to serpentinite, which has high Mg and low Al contents, and to the sedimentary rocks, which have relatively low Mg and high Al contents. Note the ~100 μm long wisp of shale at the tip and the tongue of shale that is nearly separated from the clast at the side (Fig. 5A and B). Mg-rich clays have grown along a crack in the shale clast (Fig. 5C and D).

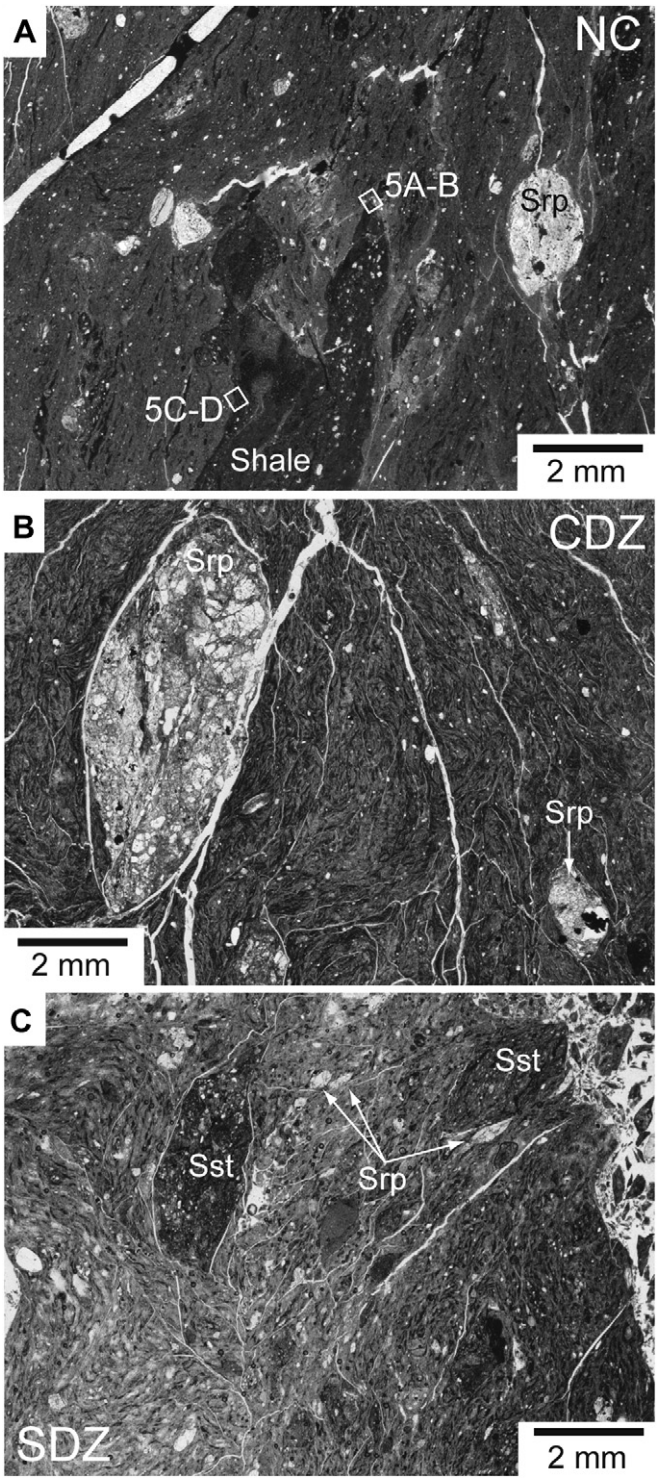

Fig. 3. Portions of thin section scans of gouge samples from (A) NC outcrop; (B) CDZ at 3297.5 m MD; (C) SDZ at 3197.7 m MD. Porphyroclasts in all gouge samples consist predominantly of serpentinite (Srp) and sedimentary rocks such as shale and siltstone (Sst). The two boxes in (A) mark the locations of the X-ray maps of Fig. 5.

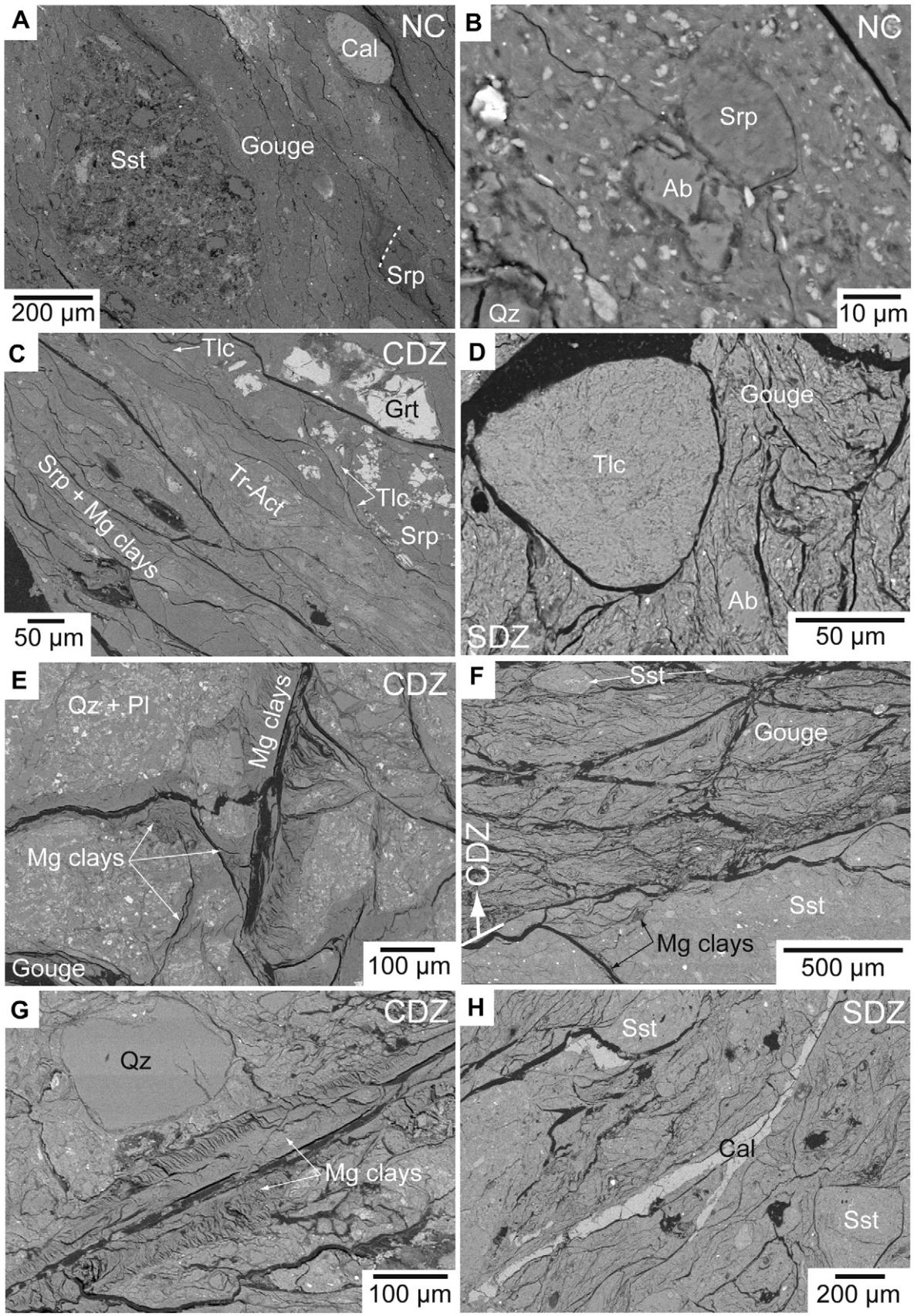

Fig. 4. Textures of gouge samples, imaged by backscattered-electron SEM techniques. (A) Aligned porphyroclasts of siltstone (Sst), serpentinite (Srp), and calcite (Cal) in NC gouge. The serpentinite clast is slightly offset along a fracture (dashed white line). (B) Fine-grained matrix of NC gouge is also rich in serpentine and sedimentary grains. Small bright grains are calcite. Ab = albite; Qz = quartz. (C) Talc (Tlc), tremolite-actinolite (Tr-Act), andradite garnet (Grt), and chlorite occur as alteration minerals in the large serpentinite clast from the CDZ shown in Fig. 3B. The outer edge of the clast contains some Mg clays (lower left). (D) Rounded porphyroclast of talc schist in the SDZ. (E) Portion of a heavily fractured quartz- and plagioclase (Pl)-rich porphyroclast in the CDZ; fractures are lined with Mg clays. (F) Siltstone-CDZ gouge contact at 3296.6 m MD. Fractures in the siltstone at the contact are filled with the same Mg clays as those in the gouge matrix. Fragments of the siltstone occur as clasts in the gouge matrix. (G) Fracture-filling, Mg-rich smectitic clays in the siltstone adjoining the CDZ. (H) Veinlets of calcite along the foliation in the SDZ gouge.

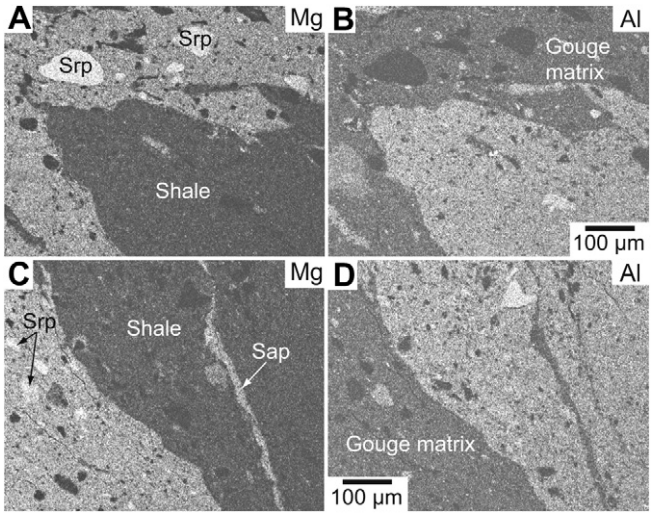

Fig. 5. Distribution of Mg and Al, obtained from SEM X-ray maps, at the boundary between the gouge matrix and the tip (A, B) and side (C, D) of the shale porphyroclast in Fig. 3A.

3.3. Clay-mineral compositions

Compositions of the matrix clays in the three gouge occurrences are presented in Supplementary Tables 1–3 and plotted in a Velde (1985) diagram in Fig. 6. Also included in Fig. 6 are two analyses of Mg clays that fill fractures in serpentinite grains from Phase 2 cuttings (Moore and Rymer, 2007). Total iron contents of the clays are treated as ferrous. In cases where closely spaced spot analyses yielded very similar compositions, those data were averaged together. Approximately 70% of the reported analyses are averages of 2–6 spots (Supplementary Tables 1–3), indicating at least some local uniformity in clay-mineral chemistry.

The clays are all Mg-rich (~22–25 wt% MgO); the ratio Mg/(Mg + Fe_{tot}) is 0.8–0.9, only slightly lower than for the associated serpentine minerals for which Mg/(Mg + Fe_{tot}) = 0.88–0.97 (Supplementary Table 4). All of the compositions lie in a band

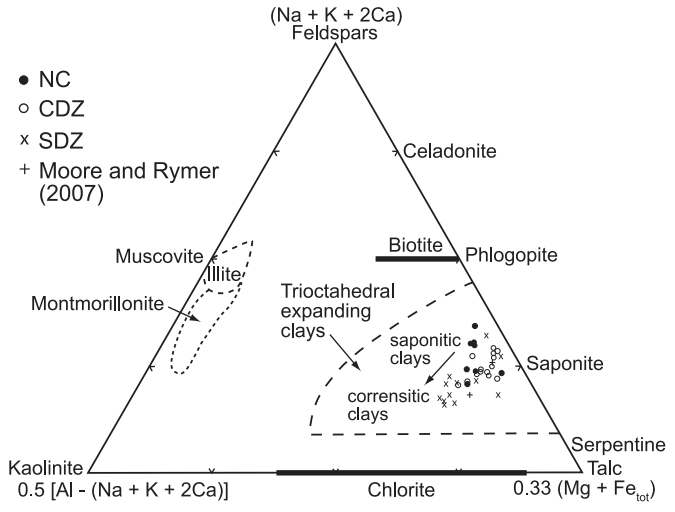

Fig. 6. Compositions of gouge-matrix clay minerals (Supplementary Tables 1-3) plotted on a Velde diagram (Velde, 1985), modified in that total Fe contents are treated as Fe^{2+}. Approximate compositional fields of illite, the dioctahedral smectite clay montmorillonite, and trioctahedral expanding clays including saponite and corrensite are from Velde (1985). Thick black lines mark the compositional ranges of biotite and chlorite.

within the field of trioctahedral expanding clays in Fig. 6 that extends from close to the end-member saponite formula about half-way towards that of chlorite. The compositions of the NC and CDZ clays plot close together on the saponite side. Some of the SDZ clays have compositions similar to those from the NC and CDZ gouges, but the majority of the SDZ clays plot closer to chlorite. The XRD patterns of the SDZ gouge samples have a peak at ~29Å (e.g., Lockner et al., 2011), indicating the presence of corrensite, a regularly interlayered, roughly 50:50 mixture of chlorite and smectite (here, saponite). The compositions of many of the SDZ clays are consistent with that. The CDZ gouges lack an obvious 29 Å peak in XRD patterns (e.g., Lockner et al., 2011), and the CDZ and NC clay compositions represent saponitic clays that contain some proportion of chlorite mixed-layers. Clay-mineral chemistry will be considered in detail in a subsequent paper.

Based on powder XRD patterns of bulk rock samples, montmorillonite was reported by Carpenter et al. (2011) in the CDZ and nontronite by Bradbury et al. (2011) in portions of the SDZ and CDZ. These are both dioctahedral smectite clays; the octahedral sites are largely occupied by Al in montmorillonite and by Fe^{3+} in nontronite. However, no evidence for the presence of these minerals was found either during SEM examination or in the microprobe data. Similarly, no trace of the illite-smectite clays described by Schleicher et al. (2010) in nearby Great Valley rocks was found amongst the matrix clays in any of the three gouges. If present, these minerals must be confined to the sedimentary porphyroclasts.

Microprobe data provide a quantitative measure of the Mg and Al concentrations illustrated qualitatively in Fig. 5. The serpentine minerals contain 37-40 wt% MgO; Al_2O_3 contents typically are ≤1 wt %, although bastites can contain ~3 wt% Al_2O_3 (Supplementary Table 4). The NC saponites average ~23 wt% MgO and 7.5 wt% Al_2O_3. The composition of the fine-grained, polymineralic matrix of the shale was estimated by averaging 22 spot analyses (the larger clasts of quartz and feldspar were avoided), which yielded ~5 wt% MgO and ~17.5 wt% Al_2O_3. In addition, silica contents of the saponites, at 41–43 wt% SiO_2, are higher on average than those of the serpentine minerals (39–42 wt% SiO_2) and lower than that of the shale matrix (~52.5 wt% SiO_2).

Bradbury et al. (2011) report whole-rock compositions of seventeen SAFOD core samples, including one each from the SDZ (3197.72 m MD) and CDZ (3298.4 m MD). Their data are consistent with the chemical differences between the shale and NC gouge matrix illustrated in Fig. 5. The two gouge samples have by far the highest Mg contents of the group, at 21.75 (SDZ) and 27.17 (CDZ) wt % MgO. With the exception of one Great Valley Group sample with 10.46 wt% MgO that is located less than 1 m southwest of the CDZ (3295.8 m MD), all of the sedimentary rocks analyzed by Bradbury et al. (2011) contain <4 wt% MgO. The SDZ and CDZ gouges also have the lowest SiO_2 (~50–55 wt%) and K_2O (~0.2–0.4 wt%) and among the lowest Al_2O_3 (~7–10 wt%) contents of the group (Table A3 of Bradbury et al., 2011).

3.4. Spinel compositions

The compositions of chromian spinels in peridotite reflect their origin (Dick and Bullen, 1984; Ishii et al., 1992) and can be used to distinguish between abyssal and forearc affinities. Relict primary spinels have also been used to infer the origin of thoroughly serpentinized ultramafic rock (Ishii et al., 1992; Saumur et al., 2010; Shervais et al., 2011). We analyzed spinels associated with serpentine in the three occurrences, to obtain information on the source(s) of the ultramafic rocks. For the NC outcrop, chrome spinels were selected from the relatively undeformed serpentinite block shown in Fig. 2A. These spinels typically are rimmed by

magnetite (Fig. 7A, Supplementary Fig. 2). From the CDZ and SDZ only those spinels that were surrounded by at least a thin shell of serpentine (Fig. 7B–C) were analyzed, to avoid possibly detrital spinels.

Ferrous and ferric iron contents of the spinel analyses reported in Supplementary Table 5 and plotted in Fig. 8 were calculated based on spinel stoichiometry. The spinels are characterized by Mg# between 52 and 68 and by Cr# in the range 38–66. The cores of the six analyzed NC spinels are essentially identical in composition, and the rim compositions differ only slightly from those of the cores (Fig. 8). Individual CDZ and SDZ spinels large enough to accommodate multiple spot analyses are also uniform in composition, but

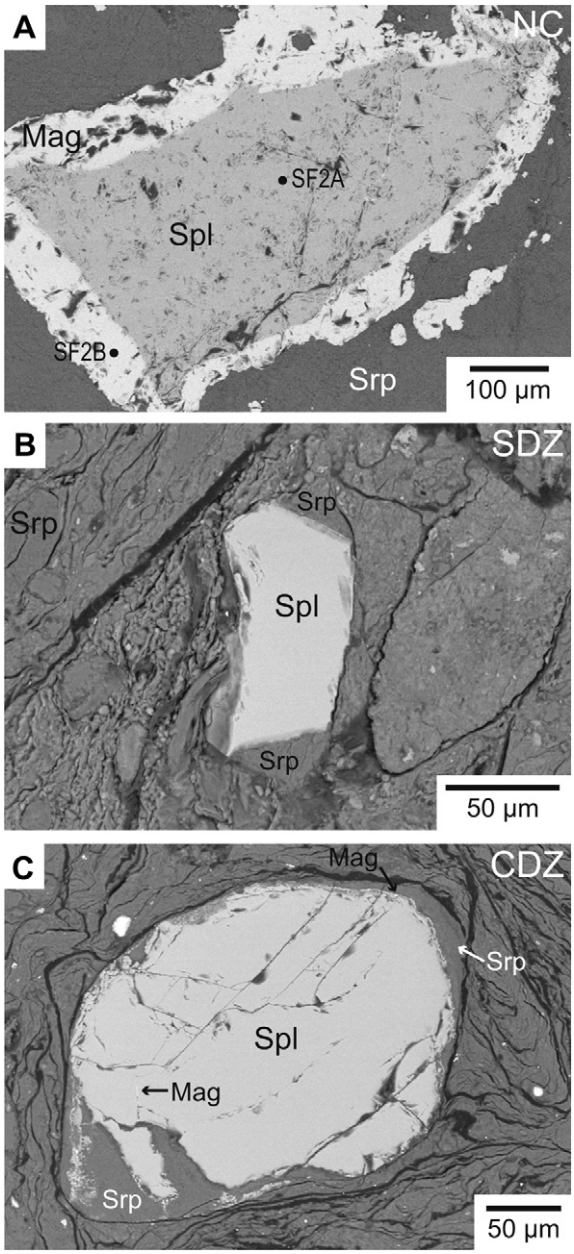

Fig. 7. Spinels from the three gouge occurrences, shown in backscattered-electron SEM images. (A) Spinel (Spl) crystal from serpentinite (Srp) of the NC outcrop; the bright rim is magnetite (Mag). The spots labeled SF2A and SF2B mark the locations of EDS spectra presented in Supplementary Fig. 2. (B) Spinel from the SDZ with fringes of serpentine at either end. (C) Spinel rimmed by serpentine in the CDZ. Traces of magnetite occur at the perimeter of the spinel crystal and along internal cracks.

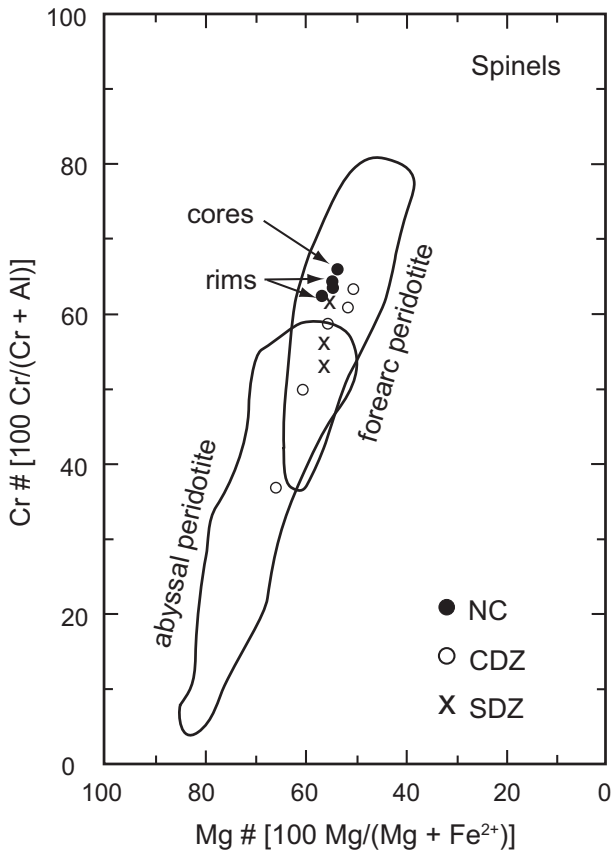

Fig. 8. Compositions of relict chromian spinels (Supplementary Table 5) in the NC serpentinite and serpentinite porphyroclasts in the CDZ and SDZ. Compositional fields were drawn by Shervais et al. (2011) from the following sources: abyssal peridotites (PetDB database) and forearc peridotites (GEOROC database).

crystal-to-crystal variations among these eight spinels are relatively large. All but one of the spinels in Fig. 6 plot well within the field of forearc peridotites, although some of the CDZ and SDZ spinels extend into the area of overlap between forearc and abyssal peridotites. The CDZ spinel with Cr# = 38 lies just outside the field of forearc peridotites.

4. Discussion

The textural and mineralogical evidence presented above demonstrate that the Nelson Creek foliated gouge has a common origin with those of the CDZ and SDZ. The Mg-rich, Al-bearing clays in all three gouges are considered to be the product of metasomatic reaction between serpentinite entrained in the fault and adjoining sedimentary rocks. Reaction occurs as a result of the marked chemical contrast between ultramafic and quartzofeldspathic rocks (e.g., Read, 1934; Phillips and Hess, 1936; Coleman, 1967; Curtis and Brown, 1969; Cooper, 1976; Koons, 1981; Sanford, 1982; Mori et al., 2007). Reaction rates may be enhanced by faulting rocks against each other in a fluid-rich environment, because shearing increases the fracturing, grain-size reduction, and intimate mixing of ultramafic and crustal rock types. This interpretation corresponds with our previous observation that the Mg-rich smectite clays replace “serpentine that has been mixed with feldspathic sediments” (Moore and Rymer, 2007, p. 797), the sediments providing Al and some Si for the clays and the serpentine providing the Mg (e.g., Fig. 5).

Spinel compositions indicate that the serpentinite associated with the Nelson Creek and SAFOD foliated gouges may represent hydrated forearc peridotite (Fig. 8). The Coast Range Ophiolite (CRO) of the California Coast Ranges is an extremely large and complex entity, but petrological and geochemical investigations of both the volcanic section (e.g., Evarts et al., 1999) and mantle peridotites (Choi et al., 2008) and their serpentinized equivalents (Shervais et al., 2011) demonstrate that it is dominantly of supra-subduction-zone origin. We therefore suggest that the serpentinite within the San Andreas Fault in the vicinity of SAFOD was derived from the CRO, rather than the oceanic lithosphere of abyssal origin upon which Franciscan sediments were deposited. One possible local source of serpentinite is the 50–60 km long and ~2 km thick slab of serpentinized ultramafic rock inferred from aeromagnetic surveys (McPhee et al., 2004), that currently is estimated to abut the SAF at ~6-km depth on the northeast side (McPhee, personal communication, 2009). Tectonic emplacement of serpentinite in faults has been reported at numerous localities in the California Coast Ranges (e.g., Page et al., 1999; Ohlin et al., 2010), including the Table Mountain serpentinite extrusion (Dickinson, 1966) located ~5 km east of Parkfield. Buoyant rise of low-density serpentinite from a deep source of CRO combined with horizontal displacement by faulting (e.g., Irwin and Barnes, 1975) may also explain the presence of serpentinite within the active SAF in this part of the creeping section. Such an emplacement mechanism would introduce a more or less continuous column of reactive serpentinite above the source tapped by the fault. This in turn would indicate a connection between the kilometers-long surface exposures of serpentinite within the fault (Fig. 1A) with one or both of the CDZ and SDZ.

The NC outcrop (Fig. 1B), dominated by serpentinite, preserves the initial stages in the development of the reaction zone. Incipient alteration of the NC serpentinite is evidenced by the loss of brucite and the precipitation of calcite in the rocks adjacent to the fault trace. At the higher P-T conditions prevailing at the depths of SAFOD core recovery, reactions have progressed to a substantially greater degree. The core recovered from the less actively deforming SDZ contains considerably larger serpentinite porphyroclasts than does the CDZ core, consistent with the idea that reaction progress is tied, at least in part, to the amount of shear.

Recent laboratory investigations by Moore and Lockner (manuscript in preparation; also Moore et al., 2010a, b) provide insights into the tectonic and chemical processes proposed here and the roles those processes play in promoting both creep and weakening. In otherwise identical experiments, serpentinite sheared against granite or quartzite under hydrothermal conditions is significantly weaker than the same serpentinite sheared against an ultramafic rock. Weakening is more pronounced at higher temperatures and slower shearing rates, the rate dependence corresponding to velocity-strengthening behavior that will promote stable slip. In contrast, serpentinite sheared in an ultramafic chemical environment becomes stronger at higher temperatures and is characterized by potentially unstable, velocity-weakening behavior at some temperature-pressure-velocity conditions (e.g., Moore et al., 1997, 2004). The cause of the weakening and stabilization of slip is interpreted to be a solution-transfer process whereby serpentine minerals are dissolved at stressed grain contacts and reprecipitated in low-stress areas. The solubility of serpentine presumably is significantly enhanced in pore fluids whose chemistry has been modified by interaction with the granite or quartzite (Moore et al., 2010b).

An inference from the laboratory experiments is that creep is initiated as soon as serpentinite is juxtaposed against crustal rocks along an active fault, although the amount of weakening observed in the experiments (to a coefficient of friction, $\mu \sim 0.3$ at 250 °C) is insufficient to explain the very low strength of the SAF. However, in a serpentinite-granite experiment lasting ~14 days, Mg-rich saponitic smectite clays crystallized on some of the boundary-shear surfaces in the serpentinite gouge. In addition, quartz and feldspar crystals in the granite adjacent to the gouge had an etched appearance caused by dissolution, and Mg-rich clays had precipitated on the etched surfaces (Moore et al., 2010b; Moore and Lockner, manuscript in preparation). Such reactions correspond to those seen in the gouge samples examined in this study (Fig. 4C, E, F, G; Fig. 5). Saponite is extremely weak ($\mu \sim 0.05$ at room temperature; Lockner et al., 2011), and as reaction proceeds and the saponite content increases the strengths of both the laboratory and natural fault zones should gradually approach that of the saponitic clay. For the SAFOD gouge samples tested by Lockner et al. (2011), $\mu \sim 0.15$. The talc-tremolite-chlorite alteration assemblage identified in the SAFOD gouge samples (Fig. 4C and D) is the higher-temperature equivalent of the saponitic alteration. While the frictional behavior of chlorite at elevated temperatures has not been studied, talc is as weak as saponite under some conditions ($\mu < 0.1$ at ~200–300 °C; Moore and Lockner, 2008).

Some of the other recent models for the origin of creep at SAFOD also emphasize the crystallization of secondary smectitic clay minerals, but in somewhat to markedly different ways from the one presented here. Holdsworth et al. (2011) noted the major differences in texture, mineralogy, and chemistry (especially the Mg-enrichment) between the gouge zones and the adjoining sedimentary units. However, they described the origin of the CDZ and SDZ in terms of highly localized alteration of the sedimentary rocks by focused fluid flow. They attributed the growth of the Mg-rich clays to migration of groundwaters that had become enriched in Mg from interaction with ultramafic rock located elsewhere (although nearby), such as, perhaps, the large body of CRO at greater depth. The model of Schleicher et al. (2010) derives from their observations of extremely thin, authigenic clay coatings, commonly illite-smectite clays, that crystallized along clast and fracture surfaces in the sedimentary damage zone rocks. Creep occurs when the "nanocoatings" of clay exceed some critical level of interconnectivity. Schleicher et al. (2010) did not examine any samples from the CDZ or SDZ, and therefore did not consider serpentinite to play any role in the origin of the clayey gouge zones or of creep.

The significance of the clayey gouge at Nelson Creek was not appreciated until the SAFOD Phase 3 core was recovered. The surface traces of other faults that juxtapose serpentinite against crustal rocks should also be examined for evidence of similar shearing-enhanced metasomatic reactions, in case such features were previously overlooked. A good place to start would be the other serpentinite-bearing faults of the San Andreas system, some of which are also characterized by fault creep (e.g., Allen, 1968; Hanna et al., 1972; Irwin and Barnes, 1975). One such example was recently identified along a creeping strand of the Bartlett Springs Fault in northern California (Moore et al., 2011). There, antigorite serpentinite has risen buoyantly within the fault through Late Pleistocene fluvial deposits and extruded onto the ground surface. Portions of the sheared serpentinite are rich in porphyroclasts containing one or more of the minerals talc, tremolite, and chlorite, and there is local development of a foliated gouge with a matrix of Mg clays whose compositions are similar to those in Fig. 6. The geologic histories of Japan and California share many common features, and Sone et al. (2012) describe laboratory studies conducted on saponite-rich gouge that was a late-stage product of the faulting of serpentinite against metasedimentary rocks along the Gokasho-Arashima Tectonic Line in Japan.

5. Conclusions

The clayey gouge in the Nelson Creek serpentinite outcrop is equivalent to and may connect with the 2 m-scale zones of foliated gouge that comprise the actively creeping strands of the San Andreas Fault at 2.65–2.7 km vertical depth in SAFOD. The serpentinite in each occurrence may represent fragments of Coast Range Ophiolite that have been tectonically emplaced from a deep source intersected by the SAF. Mechanical mixing and metasomatic reaction of silica-undersaturated serpentinite with adjoining quartzofeldspathic sedimentary rocks produced fault gouge rich in extremely weak Mg-rich clays, explaining both the low strength and the occurrence of creep, at least at shallow depths (<3 km), along the central San Andreas Fault.

Acknowledgments

The manuscript has benefitted from the comments of R. G. Coleman and W. P. Irwin and reviews by W. G. Ernst, R. C. Evarts, C. Viti and an anonymous reviewer. R. Oscarson provided technical assistance with the SEM and microprobe work. We thank the three SAFOD Principal Investigators, W. Ellsworth, S. Hickman, and M. Zoback, for their efforts in bringing the SAFOD deep-drilling program to fruition. S. Hickman has been an invaluable source of information regarding SAFOD.

Appendix. Supplementary material

Supplementary data related to this article can be found online at doi:10.1016/j.jsg.2011.11.014.

References

Allen, C.R., 1968. The tectonic environments of seismically active and inactive areas along the San Andreas fault system. In: Dickinson, W.R., Grantz, A. (Eds.), Proceedings of Conference on Geologic Problems of San Andreas Fault System. Stanford University Publications in the Geological Sciences, vol. 11, pp. 70–80.

Bradbury, K.K., Evans, J.P., Chester, J.S., Chester, F.M., Kirschner, D.L., 2011. Lithology and internal structure of the San Andreas fault at depth based on characterization of phase 3 whole-rock core in the San Andreas fault Observatory at depth (SAFOD) borehole. Earth and Planetary Science Letters 310, 131–144. doi:10.1016/j.epsl.2011.07.020.

Carpenter, B.M., Marone, C., Saffer, D.M., 2011. Weakness of the San Andreas Fault revealed by samples from the active fault zone. Nature Geoscience 4, 251–254. doi:10.1038/ngeo1089.

Chester, J.S., Chester, F.M., Sills, D.W., Heron, B., Almeida, R.V., Guilmette, R.N., 2010. Structure of the San Andreas fault at SAFOD. Eos Transactions of the American Geophysical Union 91 (52) Fall Meeting Supplement, Abstract T52B-03.

Choi, S.H., Shervais, J.W., Mukasa, S.B., 2008. Supra-subduction and abyssal mantle peridotites of the Coast Range ophiolite, California. Contributions to Mineralogy and Petrology 156, 551–576.

Coleman, R.G., 1967. Low-temperature reaction zones and alpine ultramafic rocks of California, Oregon, and Washington. United States Geological Survey Bulletin 1247, 1–49.

Cooper, A.F., 1976. Concentrically zoned ultramafic pods from the Haast schist zone, South Island, New Zealand. New Zealand Journal of Geology and Geophysics 19, 603–623.

Curtis, C.D., Brown, P.E., 1969. The metasomatic development of zoned ultramafic bodies in Unst, Shetland. Contributions to Mineralogy and Petrology 24, 275–292.

Dick, H.J.B., Bullen, T., 1984. Chromian spinel as a petrogenetic indicator in abyssal and alpine-type peridotites and spatially associated lavas. Contributions to Mineralogy and Petrology 86, 54–76.

Dickinson, W.R., 1966. Table Mountain serpentinite extrusion in California Coast ranges. Geological Society of America Bulletin 77, 451–472.

Evarts, R.C., Coleman, R.G., Schiffman, P., 1999. The Del Puerto ophiolite: petrology and tectonic setting. In: Wagner, D.L., Graham, S.A. (Eds.), Geologic Field Trips in Northern California. California Division of Mines and Geology Special Publication 119, pp. 136–149.

Hanna, W.F., Brown Jr., R.D., Ross, D.C., Griscom, A., 1972. Aeromagnetic reconnaissance and generalized geologic map of the San Andreas fault between San Francisco and San Bernardino, California. United States Geological Survey Geophysical Investigations Map GP-815.

Holdsworth, R.E., Van Diggelen, E.W.E., Spiers, C.J., De Bresser, J.H.P., Walker, R.J., Bowen, L.A., 2011. Fault rocks from the SAFOD core samples: implications for weakening at shallow depths along the San Andreas Fault, California. Journal of Structural Geology 33, 132–144. doi:10.1016/j.jsg.2010.11.010.

Hostetler, P.B., Coleman, R.G., Mumpton, F.A., Evans, B.W., 1966. Brucite in alpine serpentinites. American Mineralogist 51, 75–98.

Irwin, W.P., Barnes, I., 1975. Effect of geologic structure and metamorphic fluids on seismic behavior of the San Andreas fault system in central and northern California. Geology 3, 713–716.

Ishii, T., Robinson, P.T., Maekawa, H., Fiske, R., 1992. Petrological studies of peridotites from diapiric serpentinite seamounts in the Izu-Ogasawara-Mariana forearc, Leg 125. In: Fryer, P., et al. (Eds.), Proceeding of the ODP. Scientific Results, vol. 125, pp. 445–485. College Station, Texas (Ocean Drilling Program).

Koons, P.O., 1981. A study of natural and experimental metasomatic assemblages in an ultramafic-quartzofeldspathic metasomatic system from the Haast Schist, South Island, New Zealand. Contributions to Mineralogy and Petrology 78, 189–195.

Lockner, D.A., Morrow, C., Moore, D., Hickman, S., 2011. Low strength of deep San Andreas Fault gouge from SAFOD core. Nature 472, 82–85. doi:10.1038/nature09927.

McPhee, D.K., Jachens, R.C., Wentworth, C.M., 2004. Crustal structure across the San Andreas Fault in the SAFOD site from potential field and geologic studies. Geophysical Research Letters 31, L12S03. doi:10.1029/2003GL019363.

Moore, D.E., Lockner, D.A., Ma, S., Summers, R., Byerlee, J.D., 1997. Strengths of serpentinite gouges at elevated temperatures. Journal of Geophysical Research 102, 14,787–14,801.

Moore, D.E., Lockner, D.A., Tanaka, H., Iwata, K., 2004. The coefficient of friction of chrysotile gouge at seismogenic depths. International Geology Review 46, 385–398.

Moore, D.E., Rymer, M.J., 2007. Talc-bearing serpentinite and the creeping section of the San Andreas fault. Nature 448, 795–797. doi:10.1038/nature06064.

Moore, D.E., Lockner, D.A., 2008. Talc friction in the temperature range 25°–400°C: relevance for fault-zone weakening. Tectonophysics 449, 120–132. doi:10.1016/j.tecto.2007.11.038.

Moore, D.E., Lockner, D.A., Ponce, D.A., 2010a. Anomalously low strength of serpentinite sheared against granite and implications for creep on the Hayward and Calaveras Faults. In: Knudsen, K., et al. (Eds.), Proceedings of the Third Conference on Earthquake Hazards in the Eastern San Francisco Bay Area. California Geological Survey Special Report 219, pp. 101–113.

Moore, D.E., Lockner, D.A., Rymer, M.J., 2010b. Laboratory and SAFOD Investigations Pertaining to the Origin of Low-Strength, Creeping Faults of the San Andreas System, California, USA. European Geophysical Union Annual Meeting, Abstract EGU2010–1191.

Moore, C.E., Rymer, M.J., McLaughlin, R.J., Lienkaemper, J.J., 2011. Mineralogy of faults in the San Andreas system that are characterized by creep. Eos Transactions of the American Geophysical Union 92, Fall Meeting Supplement, Abstract V11A-2504.

Moore, D.E., Lockner, D.A., in preparation. Chemical controls on fault behavior: Marked weakening of serpentinite sheared against quartz-bearing rocks. Journal of Geophysical Research.

Mori, Y., Nishiyama, T., Yanagi, T., 2007. Chemical mass balance in a reaction zone between serpentinite and metapelites in Nishisonogi metamorphic rocks, Kyushu, Japan: implications for devolatilization. Island Arc 16, 28–39.

Mumpton, F.A., Jaffe, H.W., Thompson, C.S., 1965. Coalingite, a new mineral from the New Idria serpentinite, Fresno and San Benito Counties, California. American Mineralogist 50, 1893–1913.

Mumpton, F.A., Thompson, C.S., 1966. The stability of brucite in the weathering zone of the New Idria serpentinite. In: Proceedings 14th National Conference on Clays and Clay Minerals, pp. 249–257.

Ohlin, H.N., McLaughlin, R.J., Moring, B.C., Sawyer, T.L., 2010. Geologic Map of the Bartlett Springs Fault Zone in the Vicinity of Lake Pillsbury and Adjacent Areas of Mendocino, Lake, and Glenn Counties, California. United States Geological Survey Open-File Report 2010–1301, 32 pp.

Page, B.M., De Vito, L.A., Coleman, R.G., 1999. Tectonic emplacement of serpentinite southeast of San Jose, California. International Geology Review 41, 494–505.

Phillips, A.H., Hess, H.H., 1936. Metamorphic differentiation at contacts between serpentinite and siliceous country rocks. American Mineralogist 21, 333–362.

Read, H.H., 1934. On zoned associations of antigorite, talc, actinolite, chlorite, and biotite in Unst, Shetland Island. Mineralogical Magazine 23, 519–540.

Rymer, M.J., Tinsley III, J.C., Treiman, J.A., Arrowsmith, J.R., Clahan, K.B., Rosinski, A.M., Bryant, W.A., Snyder, H.A., Fuis, G.S., Toké, N.A., Bawden, G.W., 2006. Surface fault slip associated with the 2004 Parkfield, California, earthquake. Bulletin of the Seismological Society of America 96 (4B), S11–S27. doi:10.1785/0120050830.

Sanford, R.F., 1982. Growth of ultramafic reaction zones in greenschist to amphibolite facies metamorphism. American Journal of Science 282, 543–616.

Saumur, B.-M., Hattori, K.H., Guillot, S., 2010. Contrasting origins of serpentinites in a subduction complex, northern Dominican Republic. Geological Society of America Bulletin 122, 292–304. doi:10.1130/B26530.1.

Schleicher, A.M., van der Pluijm, B.A., Warr, L.M., 2010. Nanocoatings of clay and creep of the San Andreas fault at Parkfield, California. Geology 38, 667–670. doi:10.1130/G31091.1.

Shervais, J.W., Kolesar, P., Andreasen, K., 2005. Field and chemical study of serpentinization — Stonyford, California: chemical fluxes and mass balance. International Geology Review 47, 1–23.

Shervais, J.W., Choi, S.H., Zoglman-Schuman, M., Mukasa, S.B., 2011. Serpentinite matrix mélange: implications of mixed provenance for mélange formation. In:

Wakabayashi, J., Dilek, Y. (Eds.), Mélanges: Processes of Formation and Societal Significance. Geological Society of America Special Paper 480, pp. 1–30.

Sills, D.W., Chester, J.S., Chester, F.M., 2009. Shape preferred orientation of porphyroclasts in the active gouge zones of the San Andreas fault at SAFOD. Eos Transactions of the American Geophysical Union 90(52), Fall Meeting Supplement, Abstract T43A–2057.

Soda, Y., Takagi, H., 2010. Sequential deformation from serpentinite mylonite to metasomatic rocks along the Sashu Fault, SW Japan. Journal of Structural Geology 32, 792–802. doi:10.1016/j.jsg.2010.05.003.

Sone, H., Shimamoto, T., Moore, D.E., 2012. Frictional properties of a metasomatic saponite-rich gouge from a serpentinite-bearing fault zone in the Gokasho-Arashima Tectonic Line, central Japan. Journal of Structural Geology 38, 172–182.

Titus, S.J., DeMets, C., Tikoff, B., 2006. Thirty-five-year creep rates for the creeping segment of the San Andreas Fault and the effects of the 2004 Parkfield earthquake: constraints from alignment arrays, continuous global positioning system, and creepmeters. Bulletin of the Seismological Society of America 96 (4B), S250–S268. doi:10.1785/0120050811.

Velde, B., 1985. Clay Minerals, A physico-chemical explanation of their occurrence. Developments in Sedimentology 40.

Whitney, D.L., Evans, B.W., 2010. Abbreviations for names of rock-forming minerals. American Mineralogist 95, 185–187. doi:10.2138/am.2010.3371.

Zoback, M., Hickman, S., Ellsworth, W., 2010. Scientific drilling into the San Andreas fault zone. Eos Transactions American Geophysical Union 91 (22), 197–199.